Oxidative Phosphorylation Fueled by Fatty Acid Oxidation Sensitizes Leukemic Stem Cells to Cold

Griessinger, Emmanuel; Pereira-Martins, Diego; Nebout, Marielle; Bosc, Claudie; Saland, Estelle; Boet, Emiline; Sahal, Ambrine; Chiche, Johanna; Debayle, Delphine; Fleuriot, Lucile

Published in:
Cancer Research

DOI:
10.1158/0008-5472.CAN-23-1006

Publication date:
2023

Oxidative Phosphorylation Fueled by Fatty Acid Oxidation Sensitizes Leukemic Stem Cells to Cold

Emmanuel Griessinger[1,2], Diego Pereira-Martins[1], Marielle Nebout[2], Claudie Bosc[3,4,5], Estelle Saland[3,4,5], Emiline Boet[3,4,5], Ambrine Sahal[3,4,5], Johanna Chiche[2,6], Delphine Debayle[7], Lucile Fleuriot[7], Maurien Pruis[1], Véronique De Mas[8], François Vergez[8], Christian Récher[8], Gerwin Huls[1], Jean-Emmanuel Sarry[3,4,5], Jan Jacob Schuringa[1], and Jean-François Peyron[2]

ABSTRACT

Dependency on mitochondrial oxidative phosphorylation (OxPhos) is a potential weakness for leukemic stem cells (LSC) that can be exploited for therapeutic purposes. Fatty acid oxidation (FAO) is a crucial OxPhos-fueling catabolic pathway for some acute myeloid leukemia (AML) cells, particularly chemotherapy-resistant AML cells. Here, we identified cold sensitivity at 4°C (cold killing challenge; CKC4), commonly used for sample storage, as a novel vulnerability that selectively kills AML LSCs with active FAO-supported OxPhos while sparing normal hematopoietic stem cells. Cell death of OxPhos-positive leukemic cells was induced by membrane permeabilization at 4°C; by sharp contrast, leukemic cells relying on glycolysis were resistant. Forcing glycolytic cells to activate OxPhos metabolism sensitized them to CKC4. Lipidomic and proteomic analyses showed that OxPhos shapes the composition of the plasma membrane and introduces variation of 22 lipid subfamilies between cold-sensitive and cold-resistant cells. Together, these findings indicate that steady-state energy metabolism at body temperature predetermines the sensitivity of AML LSCs to cold temperature, suggesting that cold sensitivity could be a potential OxPhos biomarker. These results could have important implications for designing experiments for AML research to avoid cell storage at 4°C.

Significance: Mitochondrial metabolism fueled by FAO alters the membrane composition and introduces membrane fragility upon cold exposure in OxPhos-driven AML and in LSCs.

See related commentary by Jones, p. 2441

Introduction

Cells rely on two main energetic pathways: glycolysis and oxidative phosphorylation (OxPhos), also called the mitochondrial metabolism that are fueled by amino acids, monosaccharides, and fatty acid (FA) pathway-derived substrates. OxPhos-driven metabolism predicts poor clinical outcomes for patients with certain types of solid tumors and leukemia (1–3). Metabolism-modulating agents, such as CPI-613, which prevents the entry of acetyl-CoA into the tricarboxylic acid (TCA) cycle, or IACS-010759, which inhibits the mitochondria complex I, have shown promise in early-stage preclinical studies and clinical trials, either alone or in combination with other classes of agents (3–8). Here we uncover that steady-state energy metabolism at 37°C predetermines the sensitivity of blasts and leukemic stem cells (LSC) from patients with acute myeloid leukemia (AML) subjected to a low temperature (4°C) commonly used as a storage procedure. While adaptive cell signaling has been widely described for normal stem cells in whole animal models or organs subjected to hypothermia, the survival of isolated cancer cells or subpopulations of cancer stem cells subjected to cold has not been detailed nor linked to OxPhos.

Materials and Methods

Cell lines and culture conditions

Human AML cell lines were maintained in RPMI1640, with 10% FBS (Lonza), 2 mmol/L L-glutamine, 1 mmol/L sodium pyruvate, penicillin (50 U/mL), and streptomycin (50 mg/mL). TF-1 cells were supplemented with GMCSF 10 ng/mL (Peprotech). AS-E2 cells were cultured in Iscove's Modified Dulbecco's Media supplemented with 20% FBS and supplemented with EPO 5 U/mL. All cell lines were grown at 37°C with 5% CO_2, split every 2–4 days and maintained in an exponential growth phase. All AML cell lines were purchased at DSMZ or ATCC, and their liquid nitrogen stock was renewed every 2 years. These cell lines have been routinely tested for *Mycoplasma* contamination in the laboratory and monitored for metabolic drift.

Patient samples

Neonatal cord blood (CB) samples were obtained from healthy full-term pregnancies were obtained at the obstetrics departments at the Martini Hospital and University Medical Center Groningen (Groningen, the Netherlands). Bone marrow or peripheral blood samples were obtained from patients diagnosed with *de novo* AML. All human samples, including healthy CB and AML samples, were obtained with a written informed consent and protocol approval by the Ethical

[1]Department of Experimental Hematology, University Medical Center Groningen, University of Groningen, Groningen, the Netherlands. [2]Université Côte d'Azur, INSERM, U1065, Centre Méditerranéen de Médecine Moléculaire (C3M), Nice, France. [3]Centre de Recherches en Cancérologie de Toulouse, Université de Toulouse, Institut National de la Santé et de la Recherché Médicale, Centre National de la Recherche Scientifique, Toulouse, France. [4]LabEx Toucan, Toulouse, France. [5]Equipe Labellisée Ligue Nationale Contre le Cancer 2018, Toulouse, France. [6]Equipe labellisée Ligue Contre le Cancer, Nice, France. [7]Université Côte d'Azur, CNRS, IPMC, Valbonne, France. [8]Service d'Hématologie, Institut Universitaire du Cancer de Toulouse-Oncopole, CHU de Toulouse, Toulouse, France.

J.J. Schuringa and J.-F. Peyron contributed as co-senior authors to this article.

Corresponding Author: Emmanuel Griessinger, University Medical Center Groningen, Groningen 9700 RB, the Netherlands. E-mail: emmanuel.griessinger@gmail.com

Cancer Res 2023;83:2461–70

doi: 10.1158/0008-5472.CAN-23-1006

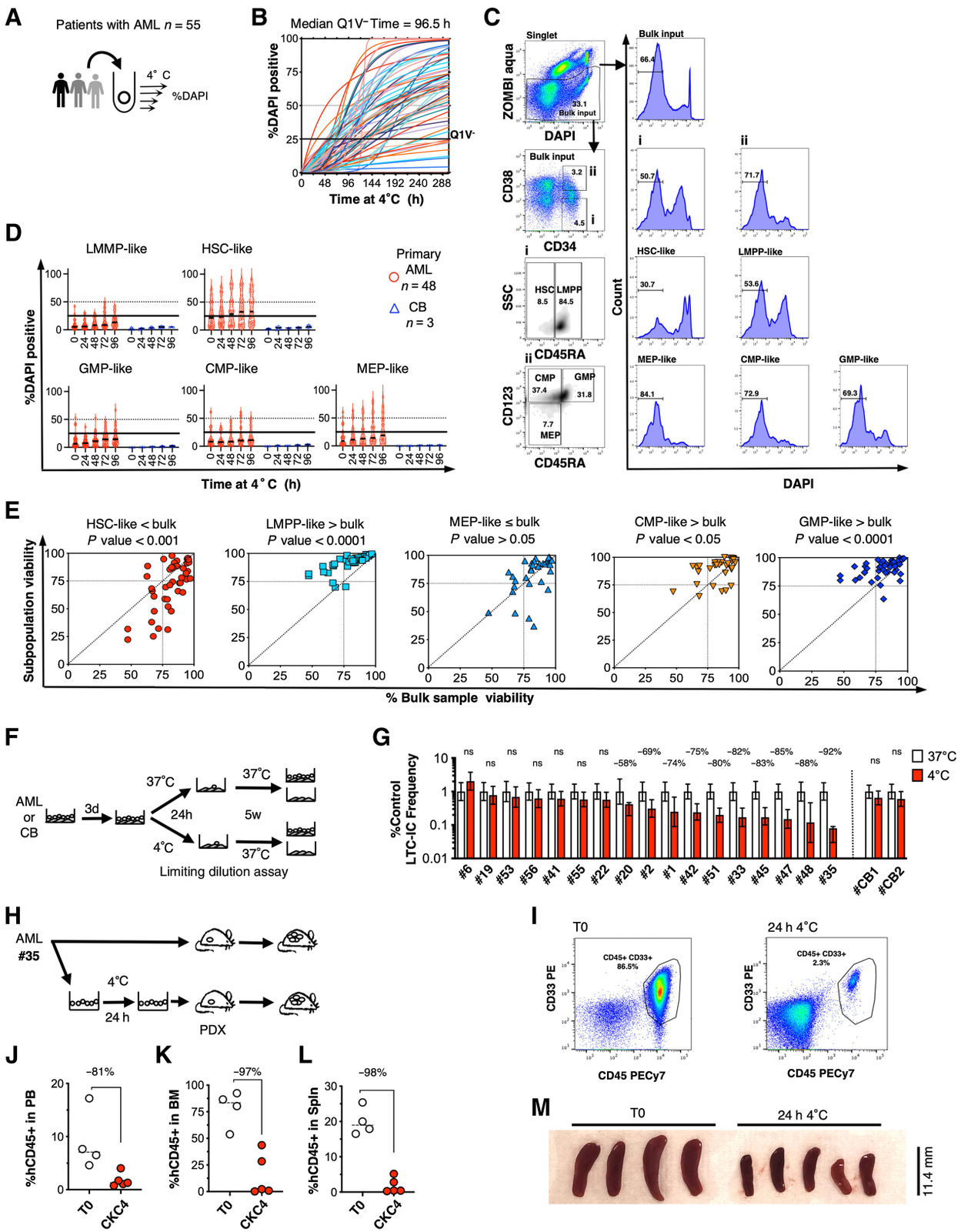

Committee in accordance with the Declaration of Helsinki. CB $CD34^+$ cells were isolated by density gradient separation, followed using a hematopoietic progenitor magnetic associated cell sorting kit (#130-046-703, Miltenyi Biotec) according to the manufacturer's instructions. All patient tissue collection and research use adhered to protocols approved by the Institutional Review Board, in accordance with the Declaration of Helsinki. Details of patient samples are listed in supplementary Supplementary Table S1. Mononuclear cells were isolated using LymphoPrep (Axis Shield Poc As) separation and cryopreserved.

Cold killing challenge at 4°C

Cells were incubated in a refrigerator calibrated at 4°C in RPMI1640, with 10% FBS, 2 mmol/L L-glutamine, 1 mmol/L pyruvate, penicillin (50 U/mL), streptomycin (50 mg/mL). Temperature was controlled for each experiment with a precision gallium thermometer. After incubation, cells were stained with DAPI (4′,6-diamidino-2-phenylindole, Invitrogen) and analyzed at room temperature by flow cytometry (FCM). For rotenone (R8875, Sigma-Aldrich), cells were treated for 10 minutes at 37°C, then washed in PBS and resuspended in a fresh medium and then incubated for the indicated time. Where indicated, glucose-free RPMI medium (Thermo Fisher Scientific) was supplemented with 5 mmol/L galactose (Sigma-Aldrich). NB-4 cells were treated with 1 μmol/L of all-trans retinoic acid (ATRA, Sigma-Aldrich) or control DMSO for the indicated time prior to cold killing challenge at 4°C (CKC4). In some experiments, cells were treated for 48 to 72 hours with etomoxir (#HY-50202, MedChem express) or Triacsin C (#ab141888, Abcam) with IC25 dose specific of each cell tested and predetermined by luciferase assay. After treatment, cells were washed with PBS, then fresh medium was added prior to CKC4.

Oxygen consumption measurement

Oxygen consumption was measured using oxygen consumption rate was measured in real time using the XF96 extracellular flux analyzer (Agilent). AML cells were seeded on Cell-Tak (#10317081, Thermo Fisher Scientific)-coated XF96 plates at 0.12×10^6 cells/well in 180 μL of XF base medium minimal DMEM (#102353-100, Agilent) supplemented with 20 mmol/L D-glucose (G6152, Sigma-Aldrich), 1 mmol/L sodium pyruvate (#11360088, Thermo Fisher Scientific), 2 mmol/L L-glutamine (#25030081, Thermo Fisher Scientific) and adjusted to pH 7.4. The plates were spun at $200 \times g$ (breaks off) and incubated at 37°C for 20 minutes to ensure cell attachment. Measurements were obtained under basal conditions and in response to mitochondrial inhibitors, 1 μmol/L oligomycin (O4876, Sigma-Aldrich), 0.5 μmol/L of carbonyl cyanide 4 (trifluoromethoxy) phenylhydrazone (FCCP, C2920, Sigma-Aldrich), and 1 μmol/L rotenone (R8875, Sigma-Aldrich) combined with 2 μmol/L antimycin A (A8674, Sigma-Aldrich).

ATP analysis

A total of 50,000 luciferase transduced cells were resuspended in 100 μL of corresponding medium supplemented with 10% FBS and distributed in a 96-well plate. Cells were then treated in triplicates for 2 hours in glucose-free medium with galactose 2 g/L to inhibit glycolysis-derived ATP, or in glucose medium with 2 μmol/L of oligomycin to inhibit OxPhos-derived ATP or in combination of both conditions to obtain the residual amount of ATP. Short-time treatment (2 hours) was chosen to avoid a metabolic switch upon inhibition of glycolysis, to reach the maximum reduction effect and to avoid cell death upon inhibition of both metabolic pathways. D-Luciferin (#122799, Perkin Elmer) was added to give a final concentration of 150 μg/mL prior to luminescence measurement. Plates were analyzed with a Luminoscan (Berthold Technologies). We verified that ATP measurements were in the linear range of the detection. The difference between total ATP production (untreated condition) and the ATP produced under glucose-free medium with galactose treatment results in glycolytic ATP. The difference between total ATP production and the ATP produced under oligomycin treatment results in OxPhos ATP contribution. OxPhos- and glycolytic-derived ATP are represented by the percentage of total ATP produced by the cells.

FCM analysis

FCM analyses were performed using MACSQuant, MACSQuant VYB or MACSQuantX analysers (Miltenyi Biotec) or LSRFortessa or CytoFLEX flow cytometer. To distinguish the initial high cellular death inherent to the thawing of primary AML cells, mononuclear cells were prestained with the dead cell–specific amine-reactive fluorescent nonleaking dye Zombie Aqua. Human hematopoietic cells were first stained with Zombie Aqua (#423101, BioLegend) following the manufacturer's instructions. After washing, cells were stained with CD45-APC-Cy7 (#304014, BioLegend), CD34-PE (#345802, BD Biosciences), CD38-APC (#303510 BioLegend), CD123-PECy7 (#560826 BD Biosciences), CD45RA-FITC (#304106 BioLegend) antibodies. DAPI was added at room temperature prior to FCM analysis. The negative fraction was determined using appropriate isotype antibodies and live population control. For measuring mitochondrial potential at 37°C or mitochondrial permeability at 4°C, cells were stained with 1 μmol/L of tetramethylrhodamine, ethyl ester, perchlorate (#87917,

Figure 1.

LSCs are sensitive to 4°C. **A,** *De novo* primary AML samples ($n = 55$; see Supplementary Table S1) were incubated at 4°C and their viability were sequentially monitored over time by DAPI incorporation staining. **B,** Kinetics of viability of primary bulk AML during the CKC4. Median value of time to lose the first quartile of viability at 4°C ($Q1V^-$ Time) determined for 55 AML samples. Curves show the experimental-derived nonlinear regression trend line determined from 5 to 7 endpoint measurements. **C,** FCM gating strategy. Input dead cells at thawing were excluded by Zombi-aqua negative selection to define the bulk leukemic population (Bulk input). Stem/progenitor-like (i, $CD34^+$ $CD38^-$) and progenitor-like (ii, $CD34^+$ $CD38^+$) were subdivided in HSC-like ($CD34^+CD38^-CD45RA^-$), LMPP-like ($CD34^+CD38^-CD45RA^+$), committed CMP-like ($CD34^+CD38^+CD45RA^-CD123^+$), GMP-like ($CD34^+CD38^+CD45RA^+CD123^+$), and MEP-like ($CD34^+CD38^+CD45RA^-CD123^-$). The DAPI fluorescence profile was then monitored at different time for the bulk input, the stem/progenitor, the progenitor, the HSC, LMPP, CMP, GMP and the MEP-like gated populations. **D,** Kinetics of viability of LMPP-like, HSC-like, GMP-like, CMP-like, and MEP-like population subset within AML and CB samples during CKC4. **E,** Subpopulation viabilities (*y*-axis) against bulk population viability (*x*-axis) in primary AML samples. Data show the viability paired comparison determined for $n = 32$ to 48 AML samples incubated at 4°C for 24 hours. Similar data were obtained at 48 and 72 hours. Comparisons were made using a paired Student *t* test. **F,** Experimental design for **G**. After 3 days of coculture with MS-5, primary AML or CB $CD34^+$ cells were either maintained at 37°C or incubated at 4°C for 24 hours, then replated in limiting dilution analysis. Then the frequency of L-LTC-IC was determined after 5 weeks of culture at 37°C. **G,** CKC4 impact on leukemic or normal LTC-IC. **H,** Xenograft assay of primary AML cells undergoing or not a CKC4 for 24 hours. **I,** Representative flow cytometric analyses in mouse recipients of sample #35 from control condition (left) or CKC4 condition (right) are shown, indicating percentages of engrafted human AML cells ($CD45^+CD33^+$) in total bone marrow cells at 10 weeks. **J–L,** Quantification of leukemic cells infiltration in PB (**J**), in the BM (**K**), and spleen (**L**) of AML #35. Each dot represents one transplanted mouse. **M,** Spleen size. For **F** and **I–K,** a Mann–Whitney *t* test was used for statistical analysis; the calculated percentage reductions are shown; bars represent median.

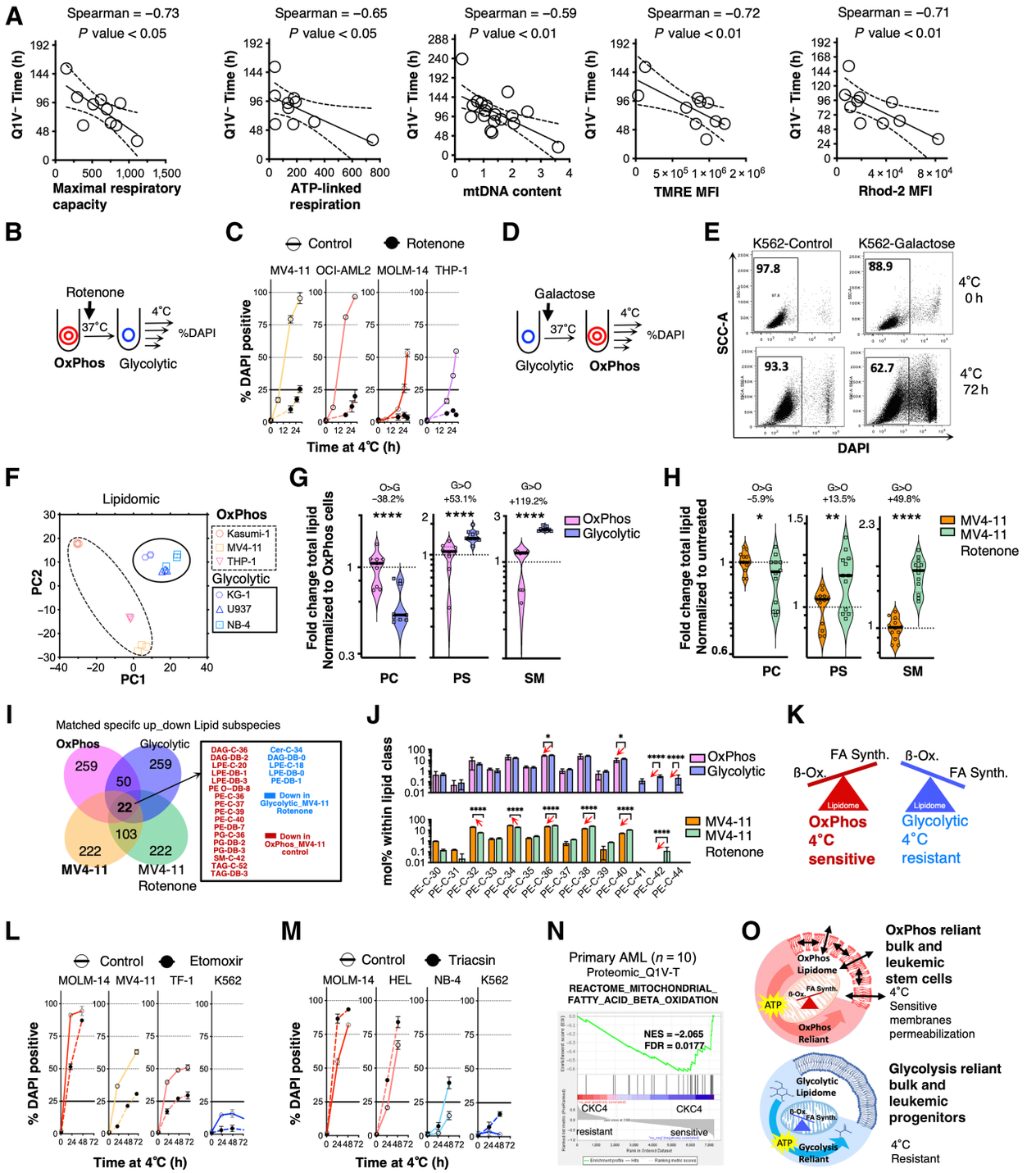

Figure 2.

OxPhos leukemic cells have a 4°C-sensitive–specific lipidome dependent on FA metabolism. **A,** Maximal respiratory capacity, ATP-linked respiration, mtDNAc, median fluorescence intensity (MFI) for the mitochondrial potential probe TMRE, and the mitochondrial calcium probe Rhod-2 as a function of Q1V⁻ Time at 4°C for primary AML. Respiration was measured with Seahorse assays under basal and maximal conditions. The relative mtDNA copy number was calculated relative to a reference DNA sample (healthy donor) set to 1. Nonparametric Spearman correlation tests were applied for $n = 10$ to 18 pairs. Thin black line shows experimentally derived linear regression trend line with 95% confidence band. **B,** Glycolytic-forced cells submitted to CKC4. Mitochondrial respiration was impaired by the complex I inhibitor rotenone. **C,** Kinetic of viability of pre-rotenone or untreated control AML cells at 4°C. **D,** OxPhos-forced cells submitted to CKC4. K562 cells were incubated at 37°C in glucose-free medium with galactose for 72 hours. **E,** Representative FACS dot plot of side scatter against DAPI for untreated control or galactose pretreated K562 cells after 72 hours at 4°C. (*Continued on the following page.*)

TMRE, Sigma-Aldrich) for 30 minutes at 37°C. For FCM analyses were performed with FlowJo software (TreeStar). Hematopoietic stem cell (HSC)-, lymphoid-primed multipotent progenitors (LMPP)-, megakaryocyte-erythroid progenitors phenotype (MEP)-, common myeloid progenitors (CMP)-, and granulocyte-macrophage progenitors (GMP)-like gates enclosing less than 300 events were excluded for viability analysis.

Mass spectrometry data acquisition

Samples were analyzed by direct infusion on a QExactive mass spectrometer (Thermo Fisher Scientific) equipped with a TriVersa NanoMate ion source (Advion Biosciences). Samples were analyzed in both positive and negative ion modes with a resolution of Rm/z = 200 = 280,000 for mass spectrometry (MS) and Rm/z = 200 = 17,500 for MS-MS experiments, in a single acquisition. MS-MS was triggered by an inclusion list encompassing corresponding MS mass ranges scanned in 1 Da increments. Both MS and MS-MS data were combined to monitor cholesterol esters (CE), diacylglycerol (DAG), and triacylglycerol (TAG) ions as ammonium adducts; phosphatidylcholine (PC), PC O-, as acetate adducts; and CL, PA, ether-phosphatidylethanolamine (PE), ether-phosphatidylethanolamine (PE O-), phosphatidylglycerol (PG), PI, and phosphatidylserine (PS) as deprotonated anions. MS only was used to monitor LPA, lyso-phosphatidylethanolamine (LPE), ether-lyso-phosphatidylethanolamine (LPE O-), LPI, and LPS as deprotonated anions; Cer, HexCer, sphingomyelin (SM), phosphatidylglycerol (LPC), and ether-lyso-phosphatidylcholine (LPC O-) as acetate adducts.

Long-term culture

Coculture experiments were performed as bulk culture or using a limiting dilution analysis both on a confluent monolayer of MS-5, supplemented with recombinant human IL3, GCSF, and TPO (MS-5 + 3GT; 20 ng/mL each; Peprotech) in Gartner's medium consisting of αMEM (Thermo Fisher Scientific) supplemented with 12.5% heat-inactivated FBS (Lonza), 12.5% heat-inactivated horse serum (Invitrogen), 1% penicillin and streptomycin, 2 mmol/L glutamine (all from PAA Laboratories).

Xenograft assay

NOD-SCID common γ-chain knockout mice (NSG mice) were purchased from the Centrale Dienst Proefdieren breeding facility within the University Medical Center Groningen (Groningen, the Netherlands). Mouse experiments were performed in accordance with national and institutional guidelines, and all experiments were approved by the Institutional Animal Care and Use Committee of the University of Groningen. Healthy 6 to 8 weeks old female mice received a single intravenous injection of 1.4×10^6 DAPI negative primary AML cells (sample #35) at T0 or 24 hours after CKC4. Animals were sacrificed 10 weeks after injection and cells from mouse peripheral blood (PB), bone marrow (BM), and spleen (Spl) were isolated. Leukocytes were recovered after red cells lysis with ammonium chloride. Cells were stained with human-specific APC–conjugated anti-CD19, PE-conjugated anti-CD33, PE-Cy7–conjugated anti-CD45 (all from BD Pharmingen). AML engraftment was defined by the presence of a single $CD45^+CD33^+CD19^-$ population.

Statistical analysis

Data presented are either a mean of triplicates samples from one representative experiment reproduced independently or a grand mean of mean response of up to 11 merged independent experiments themselves made in triplicates. Data were analyzed for statistical significance using the Mann–Whitney unpaired two-tailed test or the one-way ANOVA test. A nonparametric Spearman test was applied for correlation. Spearman rank correlation coefficient (?) is shown. Observed differences were regarded as statistically significant if the calculated two-sided P value was below 0.05. When a correlation was proven, a linear or nonlinear regression trend lines were performed with GraphPad Prism software (v9.5.0).

Data availability

The data generated in this study are available in the article and its Supplementary Data. Additional data are available upon request from the corresponding author.

Results

Interpatient and intrapatient cold sensitivity heterogeneity

Primary AML patient samples (Supplementary Table S1) incubated in culture medium at 4°C significantly lose their viability over time as evidenced by an increased positivity to DAPI staining when the cells have regained their normothermia (**Fig. 1A** and **B**). While some samples were highly sensitive to death induced by the CKC4, others appeared resistant. Analysis of CKC4 responses revealed that the time to lose the first quartile of the viability of the population ($Q1V^-$ Time) was an efficient early and simple parameter allowing to rank the cold sensitivity. A strong variation in $Q1V^-$ Time between AML samples was observed, ranging from 4 to 300 hours with a median value of 96.5 SEM ±7.14 hours. AML with a high $Q1V^-$ Time had a significantly higher white blood count (OR: 6.9; $P = 0.034$) and harbored almost four times more the FMS-like tyrosine kinase-3 internal tandem duplication (OR: 3.75; $P = 0.034$) or *NPM1* mutations (OR: 4.5; $P = 0.04$; Supplementary Fig. S1A). No difference in 4°C sensitivity was seen for patient age or risk groups or response to treatment. Similar heterogeneity in cold sensitivity was observed with a panel of 21 commonly used human myeloid or lymphoid leukemic cell lines (Supplementary Fig. S1B and S1C). We questioned whether LSCs would also be sensitive to 4°C. We monitored

(*Continued.*) **F,** Principal component analysis score plot of the total lipidome by MS (including species and subspecies analysis) of three OxPhos (Kasumi-1, THP-1, MV4-11) and three glycolytic leukemic cells (KG-1a, NB-4, U937), triplicate per cell type. **G,** Fold change of ether-phosphatidylcholine (PC), phosphatidylserine (PS), and sphingomyelin (SM) for OxPhos (O), and glycolytic cells (G) as indicated, normalized to the mean percentage for OxPhos cells (see also **Table 1**; Supplementary Fig. S2I). **H,** Fold change of PC, PS, and SM for untreated OxPhos MV4-11 and glycolytic reprogrammed rotenone-treated MV4-11 cells. **I,** Venn diagram of significantly different proportion of lipid subspecies for OxPhos and glycolytic cells cohorts and for MV4-11 and MV4-11 rotenone-treated cells (see also **Table 2**). **J,** Repartition of PE-C-30 to PE-C-44 subspecies within the PE family for OxPhos and glycolytic cells cohorts and for MV4-11 and MV4-11 rotenone-treated cells. **K,** Diagram showing the hypothesis tested in **L** and **M**. **L** and **M,** Indicated cells were pretreated with nontoxic dose of mitochondrial β-oxidation inhibitor etomoxir (**L**) or with lipid synthesis inhibitor Triacsin C (**M**) for 72 hours before undergoing a CKC4. **N,** Total proteome by MS for 10 patient samples. Pearson correlations were calculated for all quantified proteins versus $Q1V^-$ Time determined, and a ranked list of Pearson coefficients was used to perform GSEAs (see also Supplementary Table S2). GSEA of FA β-oxidation in CKC4-resistant versus CKC4-sensitive primary AML samples. **O,** Overview of study findings. OxPhos-reliant blast and LSCs cells have a FA-specific metabolism, shaping the composition of their membranes and accounting for their faster permeabilization compared with glycolysis-dependent leukemic blasts and progenitors. Mann–Whitney test was applied. *, $P < 0.05$; **, $P < 0.01$; ****, $P < 0.0001$.

the respective sensitivity to cold exposure of leukemic subpopulations bearing the hematopoietic stem cell phenotype (HSC-like; $CD34^+CD38^-CD45RA^-$), the LMPP-like ($CD34^+CD38^-CD45RA^+$), the committed CMP-like ($CD34^+CD38^+CD45RA^-CD123^+$), the GMP-like ($CD34^+CD38^+CD45RA^+CD123^+$), and the MEP-like ($CD34^+CD38^+CD45RA^-CD123^-$; **Fig. 1C**; refs. 9–11). Eight AML samples that were CD34-negative were excluded. We evidenced for 48 samples that HSC-like AML cells were more sensitive to CKC4 as compared with their normal counterpart measured in CB samples or compared with MEP-like, CMP-like, GMP-like, and LMPP-like AML cells (**Fig. 1D**). The sensitivity to CKC4 of HSC-like AML cells was independent of the initial bulk viability after thawing at different measurement times (**Fig. 1E**). We also noticed that the bulk sensitivity did not depend on the abundance of the HSC-like cells, which suggests that the loss of viability results from the cumulative sensitivity of different populations. Thus, cold sensitivity reveals differences between samples and between sample subpopulations.

LSC are sensitive to 4°C

LSCs can harbor membrane markers different from normal HSCs (11). Thus, we tested functionally how the CKC4 could impair the leukemic long-term culture initiating cells compartment (L-LTC-IC) that we have previously shown to be a faithful read-out for functionally defined LSC (12). We chose a 24-hour incubation period at 4°C, four times lower than the $Q1V^-$ Time median of our cohort to fairly estimate the sensitivity of the LSCs. Seventeen AML samples and two CB samples were incubated either at 4°C or at 37°C for 24 hours, then frequencies of LTC-IC were determined at 37°C for both conditions (**Fig. 1F**). No significant count differences were seen at the bulk population level after 24 hours at 4°C for AML and CB. However, for 10 AML samples out of the 17 tested (58%) a reduction in the frequency and the absolute number of L-LTC-IC was observed after CKC4 ranging from 58% to 92% reductions as compared with the constant 37°C experimental arm (**Fig. 1G**). No 4°C impact was seen for the CB samples tested. We tested the CKC4 impact at the level of the SCID leukemia-initiating cells (SL-IC) through the xenograft assay (**Fig. 1H**). Because in the in LTC experiments, the control experimental arm maintain at 37°C arm may have benefit from a transient expansion we decided for SL-IC measurement to inject an equal number of live cells at T0 or 24 hours after the CKC4. Ten weeks later, we observed a massive reduction of patient leukemia infiltration in the mice PB, in their BM, and Spln, as well as a reduced splenomegaly in the experimental arms of the CKC4 (**Fig. 1I–M**). This clearly shows that LSCs are selectively highly sensitive to cold exposure.

OxPhos leukemic cells exhibit a specific membrane permeabilization at 4°C

We noticed that CKC4 sensitivity did not correlate with freeze/thaw sensitivity, cell size, or cell division rate (Supplementary Fig. S1D–S1G). However, we evidenced that cold sensitivity depends on mitochondrial parameters measured at steady state in normothermia. We measured a significant negative correlation between the $Q1V^-$ Time parameter and the maximal and spare respiration capacity, the ATP-linked respiration, the mitochondrial DNA content (mtDNAc), the mitochondrial membrane potential, the calcium content as well as the amount of ATP generated by OxPhos (**Fig. 2A**; Supplementary Fig. S1H–S1J). CKC4 responses were highly reproducible (Supplementary Fig. S1K). Cell death at 4°C was characterized by permeabilization of the plasma membrane and the organelles membrane as evidenced by the leakage of fluorescent molecules DAPI, TMRE, or GFP, which occurred with a faster kinetic for OxPhos cells (Supplementary Fig. S1L). The cell-specific membrane permeabilization at 4°C was confirmed by either performing CKC4 on cell lines that were biobanked and maintained in different laboratories or by testing the same cells in different laboratories, resulting in similar sensitivity profiles (Supplementary Fig. S1M and S1N). Altogether, our results suggest that leukemic cells relying on OxPhos metabolism are specifically sensitive to CKC4.

The metabolic state shapes the cellular cold sensitivity

Because enzymatic activities are impeded at 4°C, we hypothesized that the metabolism at 37°C predetermines the sensitivity to CKC4. We wondered whether we could modify the CKC4 response by directly influencing the metabolic state at 37°C prior to cold exposure. We identified different OxPhos-dependent cell lines that tolerated the blockade of the mitochondrial complex I by rotenone and were consequently driven into glycolysis, as evidenced by an increased lactate secretion (MOLM-14, MV4-11, OCI-AML2, THP-1; **Fig. 2B**; Supplementary Fig. S2A). These glycolytic-forced cells became CKC4 resistant (**Fig. 2C**). This induced resistance required at least 24 hours of metabolic reprogramming at 37°C (Supplementary Fig. S2B). We next undertook the opposite experiment by forcing glycolytic cells to become OxPhos (**Fig. 2D**). K562 cells incubated for 72 hours with the glucose stereoisomer galactose could switch their energy production toward OxPhos (Supplementary Fig. S2C; ref. 13). Control K562 cells were cold resistant, but became sensitive upon pretreatment with galactose (**Fig. 2E**). NB4 cells can be differentiated upon treatment with ATRA, coinciding with decreased glycolysis and increased in OxPhos (Supplementary Fig. S2D and S2E). ATRA-treated NB4 became CKC4 sensitive (Supplementary Fig. S2F). And similar to what was observed during the metabolic reprogramming of OxPhos cells toward glycolysis, the OxPhos switch of NB4 cells also required a long period to influence the CKC4 response (Supplementary Fig. S2G), suggesting that sensitivity to cold exposure reflects a stable and pre-established mitochondria-dependent metabolic profile. Overall, modulating OxPhos influenced the cellular cold sensitivity, which reveals a causal relationship between the steady-state cellular metabolism and the cell death at 4°C.

OxPhos leukemic cells have a CKC4-sensitive–specific lipidome dependent on FA metabolism

We then investigated which molecular mechanisms could underlie the specific sensitivity of OxPhos cells during CKC4. We performed a Pearson correlation analysis using the $Q1V^-$ Time and a metabolomics dataset from the Cancer Cell Line Encyclopedia (14), which uncovered that many lipids had a clear abundance difference between OxPhos and glycolytic cells (Supplementary Fig. S2H). To confirm this observation, we performed a complete lipidomic analysis of three OxPhos and three glycolytic AML cell lines. The principal component analysis of 1,372 lipid subspecies confirmed a marked difference between the lipidomic profile of OxPhos and glycolytic leukemic cells (**Fig. 2F**). Eleven of the 19 classes of lipids, including energy storage and membrane lipids, were found different between OxPhos and glycolytic cells. OxPhos cells had a higher proportion of PE O-, ether-PC, TAG, DAG, PG, ceramide (CER), LPC O-, LPE O- and a lower proportion of PE, PS, and SM (**Table 1**; **Fig. 2G**; Supplementary Fig. S2I). We also determined the lipidome of OxPhos MV4-11 cells treated with rotenone for 72 hours and detected a profound lipidome remodeling upon OxPhos interference mimicking certain aspects of the glycolytic cell lipidome profile such as a lower PC and higher PS and SM content (**Fig. 2H**). A total of 22 lipid subspecies were commonly enriched or reduced between OxPhos versus glycolytic cells and between MV4-11 versus glycolytic-forced MV4-11 cells.

Table 1. OxPhos and glycolytic AML cells lipid class percentages.

	Kazumi-1 (O)	THP-1 (O)	MV4-11 (O)	KG-1 (G)	NB-4 (G)	U937 (G)	Percentage change (O-G)	Fold percentage change (O/G)	*P*
CE	0.456 ± 0.608	0.487 ± 0.032	0.12 ± 0.1545	0.821 ± 0.000	0.964 ± 0.964	0.174 ± 0.000	ns	ns	5.85E-01
Cer	0.398 ± 0.009	0.617 ± 0.011	0.294 ± 0.028	0.108 ± 0.013	0.097 ± 0.008	0.096 ± 0.003	0.336	4.340	1.09E-04
CL	0.439 ± 0.127	0.734 ± 0.074	1.226 ± 0.633	1.017 ± 0.102	0.704 ± 0.096	1.019 ± 0.048	ns	ns	5.80E-01
DAG	2.725 ± 0.061	1.783 ± 0.097	1.080 ± 0.123	0.570 ± 0.057	0.543 ± 0.024	0.840 ± 0.044	1.211	2.861	9.20E-04
HexCer	0.018 ± 0.003	0.319 ± 0.012	0.651 ± 0.110	0.115 ± 0.023	0.136 ± 0.021	0.210 ± 0.010	ns	ns	1.03E-01
LPC	0.024 ± 0.001	0.213 ± 0.008	0.086 ± 0.011	0.048 ± 0.002	0.057 ± 0.007	0.047 ± 0.001	ns	ns	7.55E-02
LPC O-	0 ± 0	0.113 ± 0.007	0.036 ± 0.024	0.016 ± 0.000	0.007 ± 0.007	0.021 ± 0.006	0.072	5.045	8.02E-03
LPE	0.022 ± 0.001	0.117 ± 0.002	0.061 ± 0.005	0.052 ± 0.008	0.063 ± 0.006	0.049 ± 0.003	ns	ns	4.00E-01
LPE O-	0.007 ± 0.000	0.036 ± 0.001	0.019 ± 0.002	0.005 ± 0.000	0.003 ± 0.002	0.004 ± 0.000	0.016	4.733	4.89E-03
PA	0 ± 0	1.317 ± 0.082	0.399 ± 0.241	0.11 ± 0.075	0.556 ± 0.042	0.393 ± 0.058	ns	ns	9.47E-02
PC	37.05 ± 1.046	42.70 ± 0.785	41.78 ± 5.067	43.82 ± 1.375	44.78 ± 0.684	43.87 ± 0.292	ns	ns	4.12E-02
PC O-	4.631 ± 0.087	6.747 ± 0.159	7.117 ± 0.844	3.180 ± 0.081	3.098 ± 0.112	5.140 ± 0.127	2.359	1.620	6.35E-04
PE	11.15 ± 0.206	10.49 ± 0.132	14.05 ± 0.399	15.89 ± 0.311	16.86 ± 0.397	14.24 ± 0.144	−3.768	0.759	7.25E-05
PE O-	8.831 ± 0.159	11.71 ± 0.147	15.09 ± 0.148	8.884 ± 0.187	7.162 ± 0.021	8.071 ± 0.238	3.837	1.477	2.60E-03
PG	0.649 ± 0.047	0.661 ± 0.023	0.819 ± 0.054	0.092 ± 0.013	0.168 ± 0.014	0.191 ± 0.005	0.559	4.717	4.91E-09
PI	8.074 ± 0.734	7.682 ± 0.663	7.253 ± 3.496	9.713 ± 0.523	9.408 ± 0.534	10.14 ± 0.935	ns	ns	4.16E-02
PS	5.474 ± 0.773	6.928 ± 0.244	5.386 ± 2.384	9.395 ± 1.511	8.893 ± 0.661	8.944 ± 0.539	−3.148	0.653	8.97E-04
SM	3.618 ± 0.069	3.538 ± 0.067	1.322 ± 0.173	6.252 ± 0.259	6.336 ± 0.336	5.995 ± 0.098	−3.368	0.456	1.02E-05
TAG	16.44 ± 0.298	3.798 ± 0.095	3.220 ± 0.477	0.463 ± 0.100	0.490 ± 0.049	0.669 ± 0.148	7.279	14.468	9.80E-03

Note: This table contains the percentage of amount of a lipid class calculated by summing the pmol values of the individual lipids belonging to each class. Class amount was then normalized to total lipid content. *P* value, Mann–Whitney *t* test was applied to compare OxPhos (O: Kasumi-1, THP-1, MV4-11) and glycolytic cells (G: KG-1, NB-4, U937).*n*=3 per cell line.

Abbreviations: CE, cholesterol esters; CER, ceramide; CL, cardiolipin; DAG, diacylglycerol; HEXCER, hexosylceramide; LPC, lyso-phosphatidylcholine; LPC (O-), lyso-phosphatidylcholine (-ether); LPE, lyso-phosphatidylethanolamine; LPE (O-), lyso-phosphatidylethanolamine (-ether); ns, not significant; PA, phosphatidate; PC, phosphatidylcholine; PC (O-), phosphatidylcholine (-ether); PE, phosphatidylethanolamine; PE (O-), phosphatidylethanolamine (-ether); PG, phosphatidylglycerol; PI, phosphatidylinositol; PS, phosphatidylserine; SM, sphingomyelin; TAG, triacylglycerol.

Table 2. Lipid subspecies enriched or reduced between OxPhos versus glycolytic and between MV4-11 versus glycolytic-forced MV4-11 AML cells.

	Kazumi-1	THP-1	MV4-11	KG-1	NB-4	U937	Fold percentage change (O/G)	*P*	MV4-11	MV4-11 rotenone	Fold percentage change (M/Mrote)	*P*
Cer-C-34	37.179	46.166	57.294	5.717	9.495	7.954	6.071	3.53E-07	57.294	52.836	1.084	4.53E-02
DAG-DB-0	6.466	37.283	17.568	4.999	7.296	7.686	3.069	1.85E-02	17.568	1.431	12.274	9.22E-04
LPE-DB-0	63.364	67.220	53.748	42.096	43.229	38.656	1.487	6.96E-06	53.748	37.052	1.451	7.14E-03
PE-DB-1	20.349	40.579	39.498	24.863	25.647	25.582	1.320	3.92E-02	39.498	26.864	1.470	1.29E-03
LPE-C-18	95.159	95.381	91.570	79.043	86.471	80.821	1.145	7.54E-03	91.570	83.679	1.094	6.89E-04
PE-C-36	26.369	31.854	23.541	30.149	33.128	28.607	0.890	3.18E-02	23.541	29.620	0.795	2.69E-05
PE-C-40	15.766	10.770	5.436	15.210	12.871	14.457	0.752	4.75E-02	5.436	11.342	0.479	5.14E-05
DAG-C-36	26.271	13.125	14.831	28.920	24.722	20.097	0.735	2.07E-02	14.831	28.772	0.515	1.35E-04
PE-C-37	1.665	0.954	0.645	1.641	1.467	1.459	0.715	2.60E-02	0.645	1.450	0.445	2.96E-02
TAG-C-52	17.219	19.072	15.408	24.181	25.972	22.511	0.711	3.89E-05	15.408	23.304	0.661	1.96E-03
LPE-DB-1	31.795	28.160	34.978	45.585	51.021	45.319	0.669	1.20E-05	34.978	40.972	0.854	4.39E-02
PE-DB-7	2.392	1.822	1.276	2.822	2.834	2.822	0.648	2.57E-04	1.276	2.802	0.455	2.03E-03
PE O-DB-8	2.226	1.286	0.908	2.589	2.346	2.030	0.635	2.35E-03	0.908	1.388	0.654	2.17E-03
DAG-DB-2	22.885	12.501	25.562	37.457	28.707	30.837	0.628	2.33E-04	25.562	32.392	0.789	7.56E-03
PE-C-39	1.097	0.448	0.172	1.132	0.791	1.009	0.586	2.38E-02	0.172	0.812	0.211	1.81E-02
PG-C-36	17.652	16.727	19.929	19.929	37.679	37.009	0.574	2.13E-03	19.929	26.827	0.743	1.10E-02
LPE-C-20	4.841	4.619	8.430	12.319	5.750	14.253	0.554	4.94E-02	8.430	16.321	0.517	6.89E-04
LPE-DB-3	4.841	4.619	8.430	12.319	5.750	14.253	0.554	4.94E-02	8.430	16.321	0.517	6.89E-04
TAG-DB-3	11.541	7.052	13.073	24.756	17.035	18.859	0.522	2.58E-05	13.073	17.807	0.734	7.33E-04
PG-DB-2	6.780	13.828	32.320	31.656	33.544	36.636	0.520	2.56E-03	32.320	47.081	0.686	1.28E-02
PG-DB-3	3.495	3.171	6.627	6.896	5.829	14.591	0.487	4.74E-02	6.627	16.300	0.407	4.79E-03
SM-C-42	21.723	12.917	5.231	27.468	35.905	30.962	0.423	2.01E-05	5.231	7.997	0.654	4.99E-02

Note: Lipid subclass amount percentages was normalized with the summing the pmol values of the individual lipids belonging to each subclass. *P* value, Mann–Whitney *t* test was applied to compare OxPhos (O: Kasumi-1, THP-1, MV4-11) and glycolytic cells (G: KG-1, NB-4, U937) and MV4-11 (M) versus glycolytic-forced rotenone-treated MV4-11 cells (Mrote). Lipid subclasses were ranked by the fold percentage change measured for O/G.

Notably, 77% of these lipid subspecies were found reduced in OxPhos cells (**Table 2**; **Fig. 2I**). Among the reduced lipids, we observed several PE subspecies (PE-C-36 to PE-C-40). PE was the second richest family of lipids representing on average 23.73% ± 2% of the total cellular lipids (**Table 1**). Among the PE family, the distribution of carbon chains of different lengths revealed that cells relying on the OxPhos metabolism have a shift toward shorter PE subspecies with an even number of carbons (**Fig. 2J**). This suggested that OxPhos leukemic cells could have higher catabolism and/or a lower anabolism of some of their FAs through the 2-carbon acetyl-CoA moiety via the FA beta-oxidation or the FA synthesis pathways, respectively, which could directly influence CKC4 response (**Fig. 2K**). We tested this hypothesis by treating leukemic cells with nontoxic doses of etomoxir, a FA beta-oxidation inhibitor that targets the mitochondrial transporter CPT-1, and Triacsin C, an inhibitor of long fatty acyl CoA synthetase, which interferes with FA synthesis. Consistently with our hypothesis, etomoxir reduced the CKC4 sensitivity while Triacsin C increased it either for OxPhos or glycolytic leukemic cells (**Fig. 2L** and **M**). To extend these results to primary AML, we established a quantitative proteome for 10 patient samples. Pearson correlations were calculated for all quantified proteins versus $Q1V^{-}$ Time (Supplementary Table S2), and a ranked list of Pearson coefficients was used to perform gene set enrichment analyses (GSEA). Consistently with our prior functional assays, this analysis identified stem cell signatures in CKC4-sensitive AML patient samples (Supplementary Fig. S2J). However, because our proteomics dataset was performed on a population of $CD34^{+}$ blasts, it is also possible that these signatures result from distinguishing between patient samples enriched in progenitors and samples enriched in more committed cells. These GSEAs also revealed that CKC4-sensitive AML patient samples were significantly enriched for the terms mitochondrial and FA β-oxidation (**Fig. 2N**), but also mitochondrial translation, pyruvate metabolism and citric acid cycle, respiratory electron transport, and oxidative phosphorylation pathways (Supplementary Fig. S2K and S2L), which confirmed the distinct mitochondrial activity measured above through functional analysis. Overall, our results show that cellular cold sensitivity is linked to a FA β-oxidation–supported OxPhos that shapes the membrane lipidome. We also reveal for the first time that cold is deleterious for L-LTC-ICs and SL-ICs (**Fig. 2O**).

Discussion

In this study, we show that leukemic cells have a distinct sensitivity to cell death induced by cold exposure and that this sensitivity is shaped by their oxidative metabolism and settled in their membrane lipid composition. Our discovery that metabolism influences the membrane composition is supported by a prior report showing changes in glycerophospholipid acyl chain lengths in yeast strains in which different kinases and phosphatases involved in energetic metabolism pathways were knocked out (15). Different studies highlighted the importance of FA metabolism and the cross-talk between LSCs and adipose tissue in the AML niche. LSCs overexpress the FA transporter CD36 and exhibit increased β-oxidation and TCA cycle activity, suggesting that LSCs likely fuel the TCA cycle and ETC with FAs from adipocytes (16–18). Recently, it has also been shown that AML cells, but not normal hematopoietic cells, provide free FAs to

mitochondria via autophagy without exogenous supply (19). Independently of the FA catabolism, enrichment of genes involved in lipogenesis has been reported within the purified subpopulation of human LSCs (20). These studies looking at lipolysis and lipogenesis support the idea that LSCs could have a different membrane composition from other leukemia cells and different from normal HSCs, which would explain the clear difference in cold sensitivity that we highlight here.

After isolation, thawing or for instance during FCM staining procedures, cells are oftentimes kept at 4°C. We have observed that some samples can lose up to 50% viability in 6 hours. In addition, we found that distinct subpopulations within primary samples, including LSCs, are even more vulnerable at 4°C than the bulk population. Beyond cell death characterized by permeabilization of the plasma membrane, it could also be that exposure to cold stimulates the differentiation of LSCs when they are returned to 37°C. Our data could explain why some primary patient samples have unexpectedly failed to engraft in immunodeficient mice following an overnight storage step at 4°C. If immediate use of the sample is not possible, the option of overnight storage at 4°C must be avoided and the samples should preferably be frozen.

Finally, although CKC4 cannot be applied to patients for direct therapeutic purposes, we believe that it could be tested in the context of autologous stem cell transplantation to selectively eradicate LSCs to avoid their reintroduction into the recipient patients. Current regulations do not provide specific information about the graft thawing method but underline that the thawing process must be carried out in the shortest possible time to bring the transplant to 37 °C. No incubation time at 4°C is used. Furthermore, our finding that OxPhos-driven AML cells and LSCs are sensitive to cold shock could possibly be extended to other blood malignancies and solid tumors and their respective cancer stem cells.

Authors' Disclosures

E. Griessinger reports grants from ERAPerMed-AML_PM, Cancéropôle PACA, and Fondation de France (00067114) during the conduct of the study; in addition, E. Griessinger has a patent for PCT/EP2020/062717 issued. M. Nebout reports grants from Fondation de France during the conduct of the study. No disclosures were reported by the other authors.

Authors' Contributions

E. Griessinger: Conceptualization, resources, data curation, formal analysis, supervision, validation, investigation, visualization, methodology, writing–original draft, project administration, writing–review and editing. **D. Pereira-Martins:** Formal analysis, validation, investigation, methodology, writing–review and editing. **M. Nebout:** Investigation. **C. Bosc:** Investigation. **E. Saland:** Investigation. **E. Boet:** Investigation. **A. Sahal:** Formal analysis, investigation. **J. Chiche:** Conceptualization, data curation, investigation, writing–review and editing. **D. Debayle:** Investigation. **L. Fleuriot:** Investigation. **M. Pruis:** Investigation. **V. De Mas:** Resources. **F. Vergez:** Resources. **C. Récher:** Resources. **G. Huls:** Resources. **J.-E. Sarry:** Resources, data curation, writing–review and editing. **J.J. Schuringa:** Resources, data curation, formal analysis, validation, writing–review and editing. **J.-F. Peyron:** Resources, data curation, funding acquisition, project administration, writing–review and editing.

Acknowledgments

The authors are indebted to patients who granted permission to use samples in research. This work is dedicated to Dr. Charles Pierre Griessinger. The authors thank the C3M core FCM Facility. E. Griessinger thanks Ruxanda Moschoi for the first "failed experiment," which sparked the development of the CKC4. Part of this work was supported by an ERAPerMed-AML_PM grant to J.J. Schuringa and by grants from the Laboratoire d'Excellence Toulouse Cancer (TOUCAN and TOUCAN2.0; contract ANR11-LABEX) and the Ligue Nationale de Lute Contre le Cancer to J-E. Sarry. J.-F. Peyron's team projects are supported by INCa (PLBio2016-162), ANR (ANR-17-CE11-0002), Fondation ARC (PJA20191209626-1), and The Sohn Conference Foundation (Sohn Monaco). The Mediterranean Centre for Molecular Medicine is supported by institutional grants from INSERM. This study was supported by a grant from the Cancéropôle PACA and the Fondation de France (00067114).

The publication costs of this article were defrayed in part by the payment of publication fees. Therefore, and solely to indicate this fact, this article is hereby marked "advertisement" in accordance with 18 USC section 1734.

Note

Supplementary data for this article are available at Cancer Research Online (http://cancerres.aacrjournals.org/).

Received April 17, 2023; revised May 24, 2023; accepted May 31, 2023; published first June 5, 2023.

References

1. Farge T, Saland E, de Toni F, Aroua N, Hosseini M, Perry R, et al. Chemotherapy-resistant human acute myeloid leukemia cells are not enriched for leukemic stem cells but require oxidative metabolism. Cancer Discov 2017;7:716–35.
2. Lee K-M, Giltnane JM, Balko JM, Schwarz LJ, Guerrero-Zotano AL, Hutchinson KE, et al. MYC and MCL1 cooperatively promote chemotherapy-resistant breast cancer stem cells via regulation of mitochondrial oxidative phosphorylation. Cell Metab 2017;26:633–47.
3. Molina JR, Sun Y, Protopopova M, Gera S, Bandi M, Bristow C, et al. An inhibitor of oxidative phosphorylation exploits cancer vulnerability. Nat Med 2018;24:1036–46.
4. Lagadinou ED, Sach A, Callahan K, Rossi RM, Neering SJ, Minhajuddin M, et al. BCL-2 inhibition targets oxidative phosphorylation and selectively eradicates quiescent human leukemia stem cells. Cell stem cell 2013;12:329–41.
5. Pardee TS, Stadelman K, Isom S, Ellis LR, Berenzon D, Hurd DD, et al. Activity of the mitochondrial metabolism inhibitor cpi-613 in combination with high dose Ara-C (HDAC) and mitoxantrone in high risk relapsed or refractory acute myeloid leukemia (AML). J Clin Oncol 33:15s, 2015 (suppl; abstr 7015).
6. M.D. Anderson Cancer Center. A phase 1 study to evaluate the safety and tolerability of IACS-010759 in subjects with advanced solid tumors and lymphoma. clinicaltrials.gov; 2020. Available from: https://clinicaltrials.gov/ct2/show/NCT03291938.
7. Subedi A, Liu Q, Ayyathan DM, Sharon D, Cathelin S, Hosseini M, et al. Nicotinamide phosphoribosyltransferase inhibitors selectively induce apoptosis of AML stem cells by disrupting lipid homeostasis. Cell Stem Cell 2021;28:1851–67.
8. Bosc C, Saland E, Bousard A, Gadaud N, Sabatier M, Cognet G, et al. Mitochondrial inhibitors circumvent adaptive resistance to venetoclax and cytarabine combination therapy in acute myeloid leukemia. Nat Cancer 2021;2:1204–23.
9. Edvardsson L, Dykes J, Olofsson T. Isolation and characterization of human myeloid progenitor populations–TpoR as discriminator between common myeloid and megakaryocyte/erythroid progenitors. Exp Hematol 2006;34:599–609.
10. Manz MG, Miyamoto T, Akashi K, Weissman IL. Prospective isolation of human clonogenic common myeloid progenitors. Proc Natl Acad Sci U S A 2002;99:11872–7.
11. Goardon N, Marchi E, Atzberger A, Quek L, Schuh A, Soneji S, et al. Coexistence of LMPP-like and GMP-like leukemia stem cells in acute myeloid leukemia. Cancer Cell 2011;19:138–52.
12. Griessinger E, Anjos-Afonso F, Pizzitola I, Rouault-Pierre K, Vargaftig J, Taussig D, et al. A niche-like culture system allowing the maintenance of primary human acute myeloid leukemia-initiating cells: a new tool to decipher their chemoresistance and self-renewal mechanisms. Stem Cells Transl Med 2014;3:520–9.
13. Rossignol R, Gilkerson R, Aggeler R, Yamagata K, Remington SJ, Capaldi RA. Energy substrate modulates mitochondrial structure and oxidative capacity in cancer cells. Cancer Res 2004;64:985–93.
14. Li H, Ning S, Ghandi M, Kryukov GV, Gopal S, Deik A, et al. The landscape of cancer cell line metabolism. Nat Med 2019;25:850–60.

15. da Silveira dos Santos AX, Riezman I, Aguilera-Romero M-A, David F, Piccolis M, Loewith R, et al. Systematic lipidomic analysis of yeast protein kinase and phosphatase mutants reveals novel insights into regulation of lipid homeostasis. Mol Biol Cell 2014;25:3234–46.
16. Samudio I, Harmancey R, Fiegl M, Kantarjian H, Konopleva M, Korchin B, et al. Pharmacologic inhibition of fatty acid oxidation sensitizes human leukemia cells to apoptosis induction. J Clin Invest 2010;120:142–56.
17. Shafat MS, Oellerich T, Mohr S, Robinson SD, Edwards DR, Marlein CR, et al. Leukemic blasts program bone marrow adipocytes to generate a protumoral microenvironment. Blood 2017;129:1320–32.
18. Ye H, Adane B, Khan N, Sullivan T, Minhajuddin M, Gasparetto M, et al. Leukemic stem cells evade chemotherapy by metabolic adaptation to an adipose tissue niche. Cell Stem Cell 2016;19:23–37.
19. Bosc C, Broin N, Fanjul M, Saland E, Farge T, Courdy C, et al. Autophagy regulates fatty acid availability for oxidative phosphorylation through mitochondria-endoplasmic reticulum contact sites. Nat Commun 2020;11:4056.
20. Xie SZ, Kaufmann KB, Wang W, Chan-Seng-Yue M, Gan OI, Laurenti E, et al. Sphingosine-1-phosphate receptor 3 potentiates inflammatory programs in normal and leukemia stem cells to promote differentiation. Blood Cancer Discov 2021;2:32–53.